

RESEARCH LETTER

10.1002/2017GL075816

Key Points:

- High-rate (1 Hz) GPS can be used to constrain earthquake predominant period
- GPS data enable us to constrain the magnitude lower bounds for earthquakes with $M_W > 7$
- The GPS-estimated predominant period can be used to supplement seismic data to reliably constrain earthquake magnitude

Supporting Information:

- Supporting Information S1
- Table S1
- Table S2

Correspondence to:

P. A. Psimoulis,
panagiotis.psimoulis@nottingham.ac.uk

Citation:



Psimoulis, P. A., Houlié, N., & Behr, Y. (2018). Real-time magnitude characterization of large earthquakes using the predominant period derived from 1 Hz GPS data. *Geophysical Research Letters*, 45. <https://doi.org/10.1002/2017GL075816>

Received 31 MAR 2017

Accepted 12 DEC 2017

Accepted article online 18 DEC 2017

Real-Time Magnitude Characterization of Large Earthquakes Using the Predominant Period Derived From 1 Hz GPS Data

Panos A. Psimoulis¹ , Nicolas Houlié^{2,3} , and Yannik Behr^{4,5} 

¹Nottingham Geospatial Institute, University of Nottingham, Nottingham, UK, ²Mathematical Physical Geodesy, Institute of Geodesy and Photogrammetry, ETH Zurich, Zurich, Switzerland, ³Seismology and Geodynamics, Institute of Geophysics, ETH Zurich, Zurich, Switzerland, ⁴Swiss Seismological Service, ETH Zurich, Zurich, Switzerland, ⁵Now at GNS Science, Wairakei, New Zealand

Abstract Earthquake early warning (EEW) systems' performance is driven by the trade-off between the need for a rapid alert and the accuracy of each solution. A challenge for many EEW systems has been the magnitude saturation for large events ($M_W > 7$) and the resulting underestimation of seismic moment magnitude. In this study, we test the performance of high-rate (1 Hz) GPS, based on seven seismic events, to evaluate whether long-period ground motions can be measured well enough to infer reliably earthquake predominant periods. We show that high-rate GPS data allow the computation of a GPS-based predominant period (τ_g) to estimate lower bounds for the magnitude of earthquakes and distinguish between large ($M_W > 7$) and great ($M_W > 8$) events and thus extend the capability of EEW systems for larger events. It has also identified the impact of the different values of the smoothing factor α on the τ_g results and how the sampling rate and the computation process differentiate τ_g from the commonly used τ_p .

1. Introduction

Seismic earthquake early warning (EEW) systems contribute toward protecting population and critical infrastructures by issuing warnings up to tens of seconds before strong shaking arrives. Real-time EEW systems have been implemented and demonstrated to have good performance for events of magnitude $M_W < 7.0$ (Allen, 2013; Allen & Kanamori, 2003; Böse et al., 2012; Espinosa-Aranda et al., 2011; Zollo et al., 2013). In order to estimate the final magnitudes of events, various strategies were based on characterizing the maximum predominant period (i.e., τ_p ; Nakamura, 1988) and the dominant period (τ_c ; Kanamori, 2005), or the displacement amplitude (i.e., P_d ; Crowell et al., 2013; Hoshiba & Iwakiri, 2011; Rydelek & Horiuchi, 2006; Wu & Zhao, 2006). However, for large events ($M_W > 7.0$), underestimation of magnitudes has been observed, likely due to the saturation of the τ_p as the smoothing factor α (i.e., $\alpha = 0.99$) masks the low-frequency contribution (Hoshiba et al., 2011; Hoshiba & Iwakiri, 2011). The most prominent example of such discrepancy has been observed during the development of the 2011 $M_W 9+$ Tohoku-oki event for which the seismic warning system initially estimated the magnitude to be $M_W \sim 7.2$ and the final estimation not exceeding $M_W 8.1$ (Hoshiba et al., 2011; Hoshiba & Iwakiri, 2011; Wright et al., 2012).

We focus here on the predominant period methodology and identify three reasons for the limited performance of EEW during large earthquakes. First is the overlap of the predominant period with microseismicity. Distant earthquakes and oceanic seismic waves (Rhie & Romanowicz, 2004, 2006; Webb, 2008) generate long-period ground motions that are well detected by EEW systems. This noise, which may include additional site-specific characteristics (McNamara & Buland, 2004), expresses the baseline noise (McNamara et al., 2009), and contributes to limitations of EEW systems in terms of both response time and magnitude determination accuracy. To overcome this issue, τ_p can be also combined with P_d for the magnitude estimation (e.g., ShakeAlert; Böse et al., 2012). Second, processing steps, such as de-trending and high-pass filtering, may remove long-period signals that are necessary to capture the size of large events (Crowell et al., 2013; Melgar et al., 2013, 2015). Third, potentially remaining errors in the acceleration record (i.e., due to microseismicity) will affect the recursive procedure of the τ_p computation (Stiros, 2008). Finally, the use of narrow-width windows, within which τ_p is computed, makes τ_p nonsensitive to long-period signals and therefore may be inappropriate to capture the seismic source spectrum of events of $M_W > 7.0$ (half-durations $dT_{50\%} > 10$ s; Meier et al., 2010; Noda et al., 2012), causing underestimation of event magnitude.

In that context, GPS waveforms may be useful to EEW systems for at least two reasons: First, GPS time series, due to their lower sensitivity (i.e., higher noise level) are able to detect only large events and therefore are not able to render the level of microseismic activity (Michel et al., 2017). GPS-based EEW systems could thus be operated continuously even before the detection of P wave. Second, GPS provides displacement time series; therefore, only differentiation is required to access velocity and acceleration information, preserving the long-period content of the waveforms processed. Weaknesses of GPS measurements, such as multipath effects or cycle slips (Houlié, Dreger, & Kim, 2014), can be limited in applications of dynamic motions, as they can be detected and removed reliably (e.g., cycle slip even in real-time applications; Banville & Langley, 2010; Momoh & Ziebart, 2012; Zhao et al., 2015) or because they have different frequency content than the seismic signal (e.g., multipath; Geng & Bock, 2013; Moore et al., 2014).

Using GPS data recorded during main shocks of magnitudes ranging between M_W6 and M_W9+ , we demonstrate that it is possible to distinguish between large (M_W6-7) and great (M_W8+) events using a GPS-based predominant period (τ_g), and to provide accurate lower bounds on the seismic moment magnitude of large events (i.e., $M_W > 8$).

2. Materials and Methods

2.1. Geodetic Data

We use GPS (1 Hz) and strong-motion (100 Hz) records of seven different earthquakes that occurred in Japan, Nepal, and the United States (Figure 1; Table S1 in the supporting information). For the two events of Tohoku-oki (M_W9+ and $M_W7.9$ aftershock), two sets of GPS time series are available:

1. Post-processed Precise Point Positioning (PPP, Ge et al., 2008; Psimoulis et al., 2014, 2015) records computed using the Bernese GPS Software 5.2 (Dach et al., 2015) and a priori information (clocks, orbit, etc.) from the Centre for Orbit Determination in Europe (Dach et al., 2009).
2. Real-time RTK mode time series computed using the Real-Time software (RTNet) and clock and orbit corrections from the VERIPOS (Rocken et al., 2011). These data were already used by Wright et al. (2012) to constrain the rupture process.

For the remaining events; $M_W6.0$ 2004 Parkfield (Houlié et al., 2014), $M_W6.0$ 2014 Napa; $M_W6.9$ 2008 Iwate, $M_W7.8$ 2015 Nepal, and $M_W8.3$ 2003 Tokachi-Oki (Houlié et al., 2011; Kelevitz et al., 2017); we used time series post-processed using the GAMIT 10.4 software (Herring et al., 2015). The processing methodology adopted focuses on modeling the phase residual after estimation of long-term ground motion parameters (Houlié et al., 2011). Such an approach has been proven to be reliable enough to successfully compare GPS time series with both seismograms and synthetic waveforms for periods ranging from 3 to 160 s (Houlié et al., 2011, 2014). Both GPS processing packages (i.e., Bernese and GAMIT) resulted in GPS time series of similar accuracy, without any impact on the τ_g estimates. However, the Bernese package was used to produce a simulated PPP real-time solution, which could be compared against the RTNet solution.

2.2. Seismic Data

For the Tohoku-oki events, τ_p was computed using KiK-net (surface sensor) and K-NET acceleration records (Aoi et al., 2011) to compare them with τ_g . We determined the P wave arrival times either by manually picking when P arrival was visible or by computing theoretical travel times using the velocity model PREM (Dziewonski & Anderson, 1981) with the TauP algorithm (<http://www.seis.sc.edu/taup>).

2.3. Predominant Period Computation

To compute the predominant period (τ_p) of a seismic signal, the accelerograms are integrated once and high-pass filtered (Butterworth filter with a cutoff frequency of 7.5 mHz) in order to minimize linear drifts of the velocity time series. At each time step i , the predominant period τ_p , (Allen & Kanamori, 2003), is computed by the recursive relation:

$$\tau_{p(i)} = 2\pi \sqrt{\frac{X_i}{D_i}} \quad (1)$$

where X_i and D_i are the smoothed squared ground velocity and acceleration, respectively, at time i , given by the relationships $X_i = \alpha X_{i-1} + x_i^2$ and $D_i = \alpha D_{i-1} + \left(\frac{dx}{dt}\right)_i^2$, with α being a smoothing constant, (Olson & Allen,

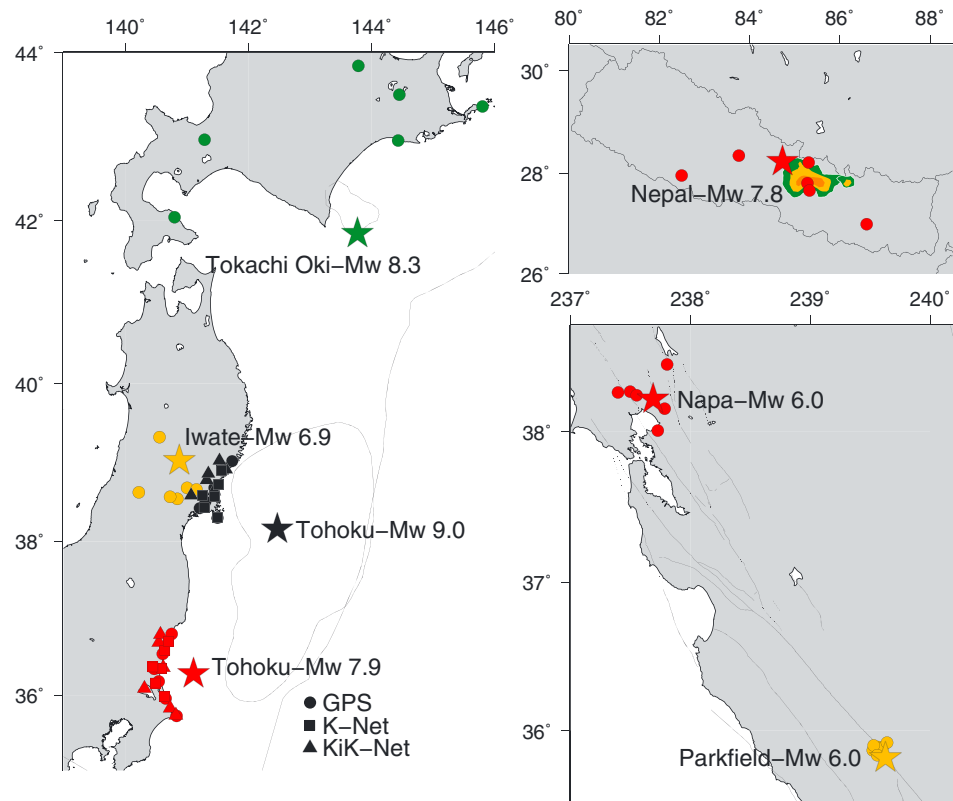


Figure 1. The GPS (circles), Kik-net (triangles) and K-NET (squares) sites selected for the estimation of τ_g value for the earthquakes of Japan, Nepal, and California. The stars indicate the epicenter of the corresponding earthquakes. The rupture of Tohoku-oki $M_W 9+$ (rupture area; Ozawa et al., 2011), Tokachi-Oki $M_W 8.3$ (rupture area; Miyazaki et al., 2004), and Nepal $M_W 7.8$ (colored scaled slip model ranging between 0 and 5 m; United States Geological Survey, 2015) are represented.

2005) taken as $\alpha = 0.99$ for 100 Hz sampling rate. The smoothing corresponds to a low-pass filter with a very gentle roll-off and an impulse response of around 10 s. The velocity time series x_i was used after passing through a 3 Hz second-order one-way low-pass Butterworth filter, a commonly followed approach to reduce the high-frequency content (Allen & Kanamori, 2003; Hoshiba et al., 2011). The τ_p^{max} corresponds to the maximum value of τ_p for the first 1 to 5 s (Olson & Allen, 2005) following the arrival of the P waves at the site (Allen & Kanamori, 2003).

3. Results

3.1. τ_g : Computation and Comparison to τ_p

For the computation of τ_g , we followed the same recursive relation of τ_p , with the GPS displacement time series being differentiated once and twice to velocity and acceleration, respectively. Using 1 Hz GPS time series and a smoothing factor α set to 0.99, results in a much longer impulse response and therefore a frequency response that focuses on longer periods than for 100 Hz data. The parameter τ_g was computed for the Up and 3-D GPS time series (Figure S1). We used the τ_g of the 3-D GPS time series as the τ_g of the Up component was more noisy, due to the higher noise level of the Up component relative to the horizontal component. In Figure 2 we present the computed τ_p of MYG011 strong-motion records and the τ_g of the GPS 0550 records, which are very closely-spaced (<100 m), for the Tohoku-Oki $M_W 9+$ earthquake. Prior to the P wave arrival, τ_p shows high values (e.g., Hoshiba et al., 2011), possibly due to the dominance of microseisms in the signal and the accumulation of errors due to the integration (Stiros, 2008). The parameter τ_g , in contrast, fluctuates around a constant noise level (Figure S1), as GPS is not sensitive enough to record microseisms and because there is no noise amplification with the differentiation procedure. After the P wave arrival, the impact of the microseisms decays, resulting in low values of τ_p (i.e., <1 s), while τ_g increases gradually,

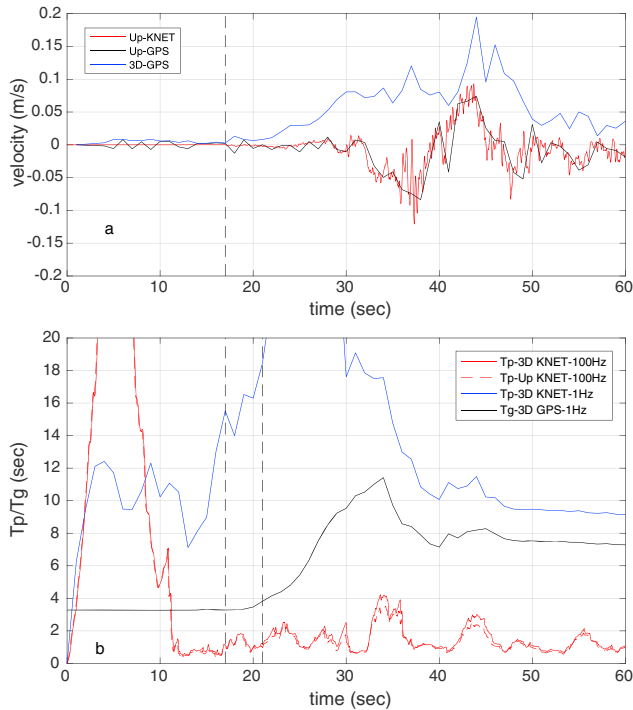


Figure 2. Time series plots of the (a) Up and 3-D velocity using the GPS site 0550 and the Up component of the velocity for the strong-motion K-NET MYG011 site, with the dotted line indicating the *P* wave arrival and (b) the τ_g value, using the 3-D time series of the GPS site, and τ_p value using the strong-motion site data of the Up component. The GPS and strong-motion sites are the closest to the epicenter of the Tohoku-oki M_W9+ earthquake. For the seismic data, τ_p is also computed using the 100 Hz and 1 Hz 3-D component time series. The time series are with respect to the start of the earthquake. The vertical dotted line indicates the 4 s time window after the *P* wave arrival, with the τ_g^{\max} corresponding to the value for $t = 4$ s (α equal to 0.99).

with the maximum value of the 4 s window after the *P* wave τ_g^{\max} , reaching 3.84 s. However, it should be stated that the 1 Hz GPS data are limited to detect predominant period larger than 2 s due to Nyquist frequency limitation.

To further investigate the difference between τ_g and τ_p , we down-sampled the seismic data to 1 Hz and calculated τ_p by following the same procedure (i.e., $\alpha = 0.99$). It is evident that τ_p still shows larger variations prior to the *P* wave arrival; however, the values show lower variation than those for τ_p of 100 Hz, due to the reduced influence of microseisms by using lower sampling rate. With the arrival of the *P* wave, and after the elimination of computation impact (i.e., $t > 30$), it shows a similar pattern as the corresponding τ_g time series with a relative offset. The latter was also confirmed through cross-correlation analysis (Figure S2). Thus, it appears that the main difference of the performance between τ_g and τ_p are the length of the impulse response function and the sensitivity to microseisms combined with the amplification of noise due to integration. For EEW based on seismic instruments, the system is required to wait for the arrival of the *P* wave to start computing a reliable τ_p time series. Otherwise, the pre-event (i.e., seismic) noise will contaminate the early part of τ_p due to the length of the impulse response. With GPS data we are able to compute predominant periods τ_g^{\max} , as the maximum value of τ_g for a time window, continuously, as the procedure of differentiation does not lead to accumulation of error and also GPS is not sensitive to seismic background noise. This removes the dependency on an accurate *P* wave detection and results overall in a much simpler procedure.

Furthermore, the τ_g time series seems to be related with the seismic motion for large earthquakes (Figure S3), reflecting the main waveform of the seismic motion, while the maximum τ_g value seems to be related with the maximum peak displacement. However, further investigation, using larger sample of seismic events and GPS sites, is

needed to analyze this correlation further as the seismic displacement is also susceptible to local site effects (landslide, etc.).

The τ_g for the Up component of GPS time series follows the same pattern as the 3-D time series; however, the noise level of τ_g for the Up component is higher than the 3-D component, making τ_g less effective (Figures S1 and S4 in the supporting information).

3.2. Smoothing Factor α

To further investigate the influence of the smoothing factor, we also used a smoothing factor of $\alpha_2 = 0.36$ in addition to the previously shown $\alpha_1 = 0.99$. The α_2 applied to 1 Hz data has the same impulse response as the α_1 applied to 100 Hz data, thus including more high-frequency signal relatively to that of α_1 for 1 Hz data.

Figure 3 shows the τ_g^{\max} time series, where each epoch i is the maximum τ_g value for the 100 s ($i - 99$ to i) and 4 s ($i - 3$ to i) window for the two smoothing factors ($\alpha_1 = 0.99$ and $\alpha_2 = 0.36$, respectively) for the six closest GPS sites of the two Tohoku-oki events (M_W9+ and $M_W7.9$ aftershock). The τ_g^{\max} time series are used to reveal the impact of the smoothing factor on the stability and the sensitivity of the τ_g computation. Results shown in Figure 3 indicate that before the *P* wave arrival, the τ_g^{\max} time series for α_2 are more scattered, defining higher noise level than the τ_g^{\max} time series for α_1 , due to the higher-frequency content. For instance, for GPS 0550, the closest GPS site for the Tohoku-oki $M9+$ earthquake, the standard deviation of the τ_g^{\max} time series are 0.03 and 0.95 for α_1 and α_2 , respectively, while the corresponding mean noise levels of τ_g^{\max} are 3.23 and 4.14, respectively. Post *P* wave arrival, τ_g also shows much less variation for α_1 than for α_2 with a clear separation between the M_W9+ and $M_W7.9$ time series.

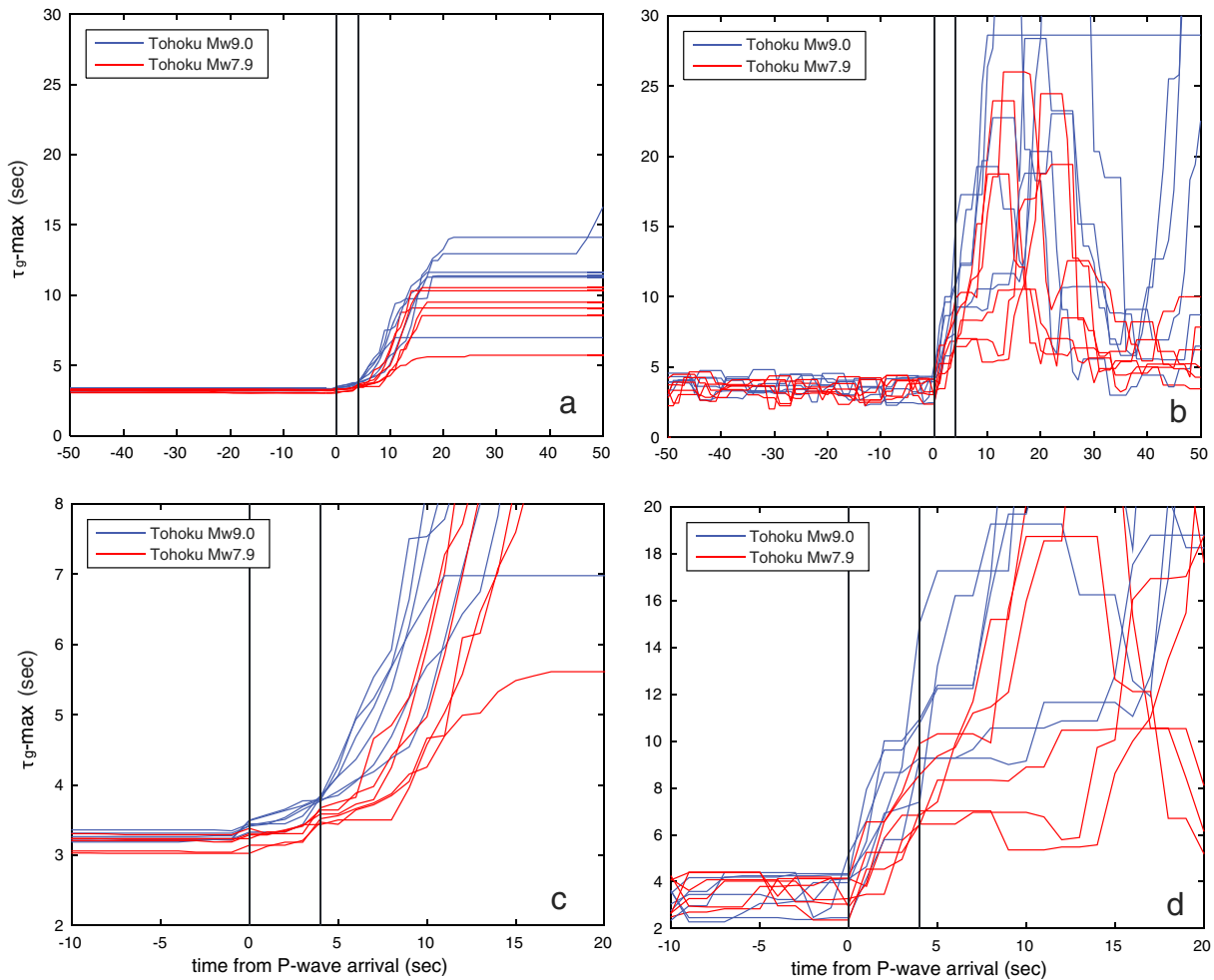


Figure 3. The τ_g^{\max} time series of the six closest GPS sites for the Tohoku-oki $M_W 9+$ earthquake (blue line) and Tohoku-oki $M_W 7.9$ aftershock (red line), with time reference to the P wave arrival, computed by using (a) $\alpha = 0.99$ with 100 s data window and (b) $\alpha = 0.36$ with 4 s data window. The two vertical lines define the 4 s time window after the P wave arrival. (c and d) Zoom on the 30 s around the P wave arrival (10 before and 20 after the P wave arrival). For relating the τ_g^{\max} time series with M_W , see Figure S7.

Such separation is less visible for α_2 , as it is more sensitive to high-frequency signal and susceptible to high-frequency measurement noise. However, for both smoothing factors the τ_g seems to differentiate roughly with the earthquake magnitude.

3.3. Statistical Significance

To test which questions could be answered in real time using τ_g^{\max} time series, we performed a series of Kolmogorov-Smirnov (KS) tests (Dimer de Oliveira, 2012; Smirnov, 1948). The two-sample KS test evaluates the hypothesis of two samples being generated from the same distribution, by returning the test result H [0,1], revealing the truth of the hypothesis and the p value [0,1], as the probability expressing the significance level of the test result on the hypothesis (Marsaglia et al., 2003). By applying the two-sample KS tests in two samples of τ_g^{\max} values, which may correspond to two different seismic events or noise, it can be assessed whether τ_g^{\max} can be used to distinguish the two events or each of them from the noise and relate them to M_W . Thus, the aim of the KS tests is to show whether τ_g^{\max} time series can be implemented and track in real-time continuous monitoring system, knowing the noise characteristic of each input time series.

3.3.1. Kolmogorov-Smirnov (KS) Test of Data Versus Noise

We first performed KS tests to check whether distributions of the noise and the data were statistically different (Tables S2 and S3) for both data windows, using the function KS test of R (Marsaglia et al., 2003). For

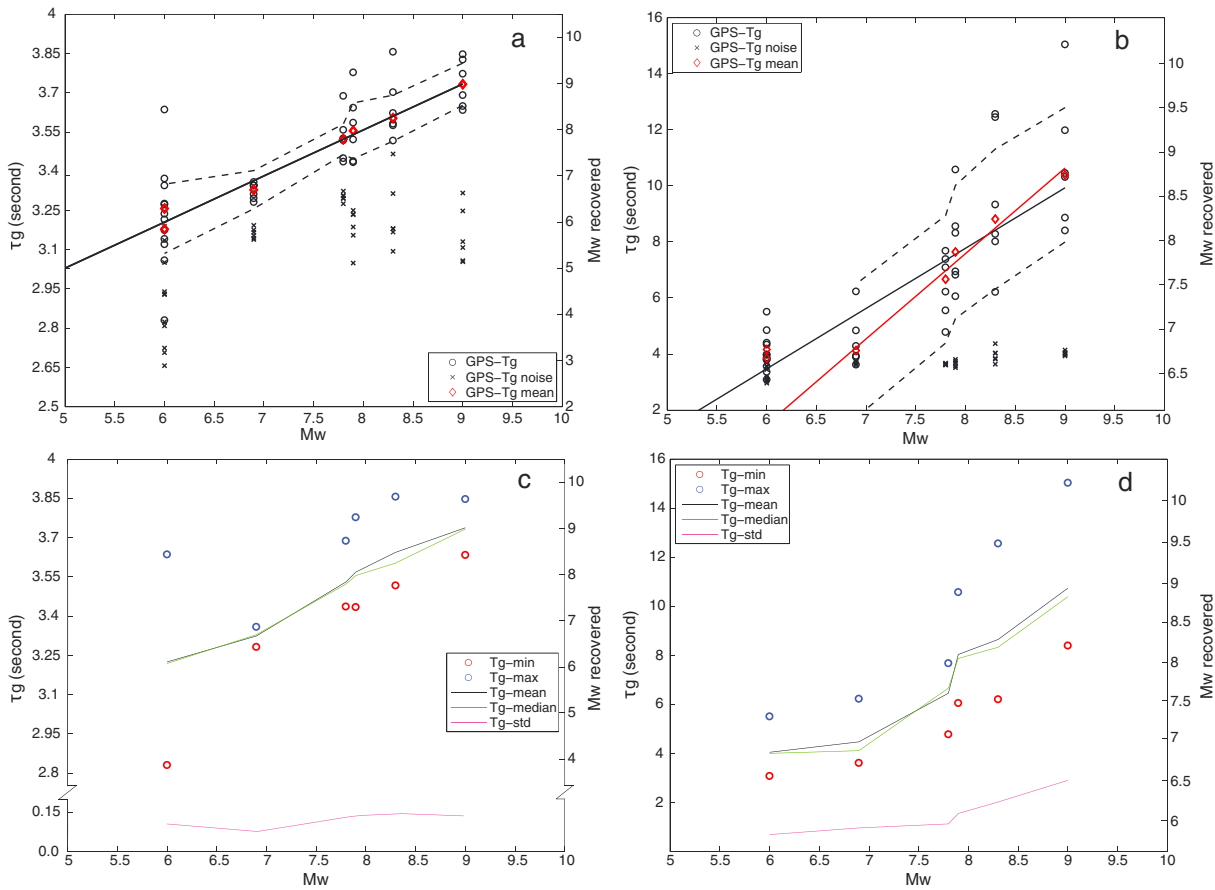


Figure 4. (top row) Semiempirical relationship between magnitude and τ_g for the postprocessed data sets (Tohoku-oki M_W 9+ 2011 and M_W 7.9 aftershock, Tokachi-Oki, 2003, Iwate 2008, Napa 2014, and Parkfield 2004) for (a) $\alpha = 0.99$ and (b) $\alpha = 0.36$. The median of each τ_g is indicated by a red diamond. The red solid line for $\alpha = 0.36$ corresponds to the linear regression by excluding the earthquakes of M_W 6.0. The dotted lines express the uncertainty level of the M_W estimates. (bottom row) Standard deviations, mean average, median, and maximum and minimum values for (c) $\alpha = 0.99$ and (d) $\alpha = 0.36$ for all τ_g measurements computed in this study. Three groups of events can be defined ($M_W < 7.0$, $M_W \geq 7.9$ –8.3, and $M_W > 8.5$).

$\alpha = 0.36$, it is not possible to differentiate data from noise for $M_W < 7.0$, while for $\alpha = 0.99$, discrimination between data estimates and background noise can be done until $M_W \sim 6.5$.

3.3.2. KS Test for Pairs of Events

We then tested the τ_g distribution for each pair of events by assessing whether these pairs are of the same distribution (Tables S4 and S5) and which set of data belong to larger earthquake (M_W of A < M_W of B; Tables S6 and S7). The success is very diverse of various events (Tables S4 and S5). The Tohoku M_W 9+ can be distinguished as the largest of all the events (<10% error). However, Tohoku-oki M_W 7.9 aftershock and Tokachi-Oki M_W 8.3 could not be distinguished (Tables S6 and S7). Nepal M_W 7.8 can be distinguished from all the events of $M_W > 7.8$ (Tables S6 and S7).

3.3.3. KS Test for Groups of Events

Statistical analysis of τ_g estimations shows that for earthquakes of $M_W < 7.0$, τ_g is very close to the noise level (Figures S5 and S6), mainly for $\alpha = 0.36$, making the estimation of earthquake magnitude less reliable.

Thus, we make three groups of events based on magnitudes: (i) $M_W < 7.0$, (ii) $M_W \geq 7.9$, and (iii) $M_W > 8.5$. To verify this hypothesis, we run a two-sample KS test for which it is possible to determine whether the distributions of τ_g values for two different groups of earthquakes are significantly different. Presented in Table S8 are the results for the comparison between groups of earthquakes of different magnitude. From the hypothesis analysis, it was verified that the Nepal earthquake M_W 7.8 can be distinguished from the earthquakes of $M_W < 7$ (i.e., Iwate, Parkfield, and Napa), while Tohoku-oki M_W 9+ can also be distinguished from the earthquakes of Tokachi-Oki M_W 8.3 and Tohoku-oki M_W 7.9 aftershock, if taken together. Finally, the Tohoku-oki M_W 9+ and Tokachi-Oki M_W 8.3 can be distinguished from the earthquakes of magnitude $M_W < 8.0$, even

though Tokachi-Oki M_W 8.3 could not be distinguished by Tohoku-oki M_W 7.9 aftershock. This is due to the distribution of Tohoku-oki M_W 9+, which makes Tokachi-Oki M_W 8.3 distinguishable from the earthquakes $M_W < 8.0$.

3.4. The τ_g^{\max} - M_W Empirical Relationship

To evaluate the relationship between τ_g and M_W , we computed τ_g^{\max} values for (i) noise (before the P wave arrival) and (ii) a 4 s window after the P wave arrival, from the six closest available GPS sites from the epicenter of each seismic event. For both smoothing factors (i.e., $\alpha = 0.36$ and $\alpha = 0.99$), the mean trend of the τ_g^{\max} increases with M_W , while the noise level of τ_g^{\max} is rather stable, regardless of the earthquake magnitude (Figures 4a and 4b). However, for $\alpha = 0.36$, the scatter and the mean trend of τ_g^{\max} values increase more rapidly with the earthquake magnitude, due to the limited impact of the smoothing on the τ_g computation (Figure 4b). Furthermore, for $\alpha = 0.36$, the τ_g values for earthquakes of M_W 6.0 are close to the noise level, as it was also revealed from the KS test, indicating that they should be excluded from the τ_g - M_W relation. Thus, by applying linear regression, we obtain the following relationship for $\alpha = 0.99$ ($M_W \geq 6$):

$$\tau_g = 0.176 M_W + 2.150 \quad (r^2 = 0.98, n = 42 \text{ and } p = 1.84 \times 10^{-5}) \quad (2)$$

and for $\alpha = 0.36$ ($M_W > 6.5$):

$$\tau_g = 3.050 M_W - 16.812 \quad (r^2 = 0.98, n = 30 \text{ and } p = 2.03 \times 10^{-3}) \quad (3)$$

where r , n , and p are the regression coefficient, the number of the data, and the p value of the regression analysis, respectively. Thus, based on the τ_g^{\max} estimates and the evaluation of their distribution for the two smoothing factors (Figures S5 and S6), we could recover the earthquake magnitude M_W . Based on the limited number of examined seismic events, the uncertainty of each M_W was computed by using the uncertainty of each estimated τ_g and the law of error propagation, resulting that for $\alpha = 0.99$ the uncertainty is ± 0.4 while for $\alpha = 0.36$ reaches up to ± 1 . Further investigation by including more seismic events is expected to limit the uncertainty of the M_W - τ_g relationship. Also, it seems that increasing the number of GPS leads to a more robust M_W estimation (Figure S8). Finally, the analysis of the statistics (i.e., maximum and standard deviation) of the τ_g^{\max} values for both smoothing factors revealed their relationship with the earthquake magnitude. The τ_g for $\alpha = 0.99$ seems to be more robust and increasing slowly with the magnitude, while the τ_g for $\alpha = 0.36$ seems to be more scattered with the latter increasing with the magnitude. However, it would be ideal to correlate the statistical characteristics of the τ_g^{\max} distribution for both smoothing factors with the earthquake magnitude, to make the magnitude estimation more robust and reliable (Figure S9).

3.5. Real Time Versus Simulated Real Time

To investigate the performance of τ_g of real-time GPS time series, we compared the τ_g estimates of the simulated real-time PPP solution against the real-time RTK solutions of the Tohoku-oki M_W 9+ earthquake. By analyzing the τ_g of the six GPS stations closest to the epicenter, we find that both sets of τ_g time series have similar patterns and amplitudes (Figures S1 and S4), resulting in consistent estimates of τ_g^{\max} . The noise level of the RTK τ_g^{\max} time series is insignificantly higher than the post-processed PPP solution (Figure S4), making the RTK time series sufficient for the reliable estimation of τ_g^{\max} . Finally, errors in real-time data can be sufficiently resolved, thanks to continuously developing methods (Momoh & Ziebart, 2012).

4. Conclusions and Discussion

We have shown that GPS can be used to constrain seismic moment M_W of large earthquakes ($M_W > 7.0$), by computing the predominant seismic period from GPS data (τ_g). The capability of GPS in recovering the period more accurately than the amplitude of the recorded motion (Häbelring et al., 2015; Moschas et al., 2014; Psimoulis et al., 2008) and the limited required filtering during the processing of GPS data (i.e., only differentiation) leads to robust and reliable estimation of τ_g without the problems of magnitude saturation due to the processing procedure (i.e., integration) of the seismic data and their sensitivity to microseismicity. The GPS τ_g estimation was computed by using two smoothing factors α (0.99 and 0.36), corresponding to low-pass filters with long- and short-period impulse responses. Even though, the smoothing factor $\alpha = 0.99$ proved to be more robust for the computation of τ_g , still the smoothing factor $\alpha = 0.36$ might be useful as its scatter

seems to depend on the earthquake magnitude. Based on that, we further established τ_g - M_W laws, which can be used to complement τ_p - M_W relationships from seismic data to reliably constrain magnitude of earthquakes $> M_W 7.0$.

Based on our data a distinction of three groups with earthquake magnitude (i) $M_W > 7.0$, (ii) $M_W > 8.0$, and (iii) $M_W > 8.5$, seems to be possible within the first 4 s of P wave arrivals. To account for rupture complexities, and the associated inability to predict the final magnitude before the end of the rupture, one could also compute a set of evolving empirical relationships based on the amount of available P wave recording (Carranza et al., 2013; Colombelli et al., 2015). The reduced noise and the potential correlation with displacement waveform, etc., make τ_g from GPS a valuable parameter in estimating the magnitude of an earthquake during or right after the rupture. However, this is only a first attempt to evaluate whether GPS records can be used for the computation of the predominant period τ_g and it is necessary to shed further light on the robustness of this method and the potential correlation of displacement waveform with τ_g , by using more GPS recordings from large earthquakes.

In conclusion, GPS-based EEW systems could be implemented and support existing seismic data-based EEW systems. The τ_g time series analyses would be routinely conducted estimating the τ_g^{\max} values for the short- and long-period smoothing factors and by calculating the corresponding statistical characteristics (e.g., mean and spread) that could provide the existing seismic warning systems with additional information to constrain the size of an earthquake of magnitude $M_W > 7$. The potential collocation of GPS and strong-motion sensors would lead potentially to even more accurate computation of the velocity through Kalman filtering (Bock et al., 2011) or other existing EEW algorithms (Benedetti et al., 2014) and enhance the performance of τ_g .

Acknowledgments

This study has been supported by Markus Rothacher and Domenico Giardini. The acquisition of GPS data of Japan has been possible due to the Swiss National Science Foundation support (SNF 200021_130061 and SNF 200021_143605). GPS data of Japan were acquired through Geographical Survey Institute (GSI) of Japan from the page http://datahouse1.gsi.go.jp/terras/terras_english.html (last accessed June 2016). RTNET 1 Hz GEONET data are provided by the Geospatial Information Authority of Japan via the Nippon GPS Data Services Company. The KiK-net and K-NET data are provided by the National Research Institute for Earth Science and Disaster Resilience (NIED). The manuscript was benefited by the comments of B. Crowell and two anonymous reviewers.

References

- Allen, R. M. (2013). Seconds count. *Nature*, *502*(7469), 29–31. <https://doi.org/10.1038/502029a>
- Allen, R. M., & Kanamori, H. (2003). The potential for earthquake early warning in Southern California. *Science*, *300*(5620), 786–789. <https://doi.org/10.1126/science.1080912>
- Aoi, S., Kunugi, T., Nakamura, H., & Fujiwara, H. (2011). Deployment of new strong motion seismographs of K-NET and KiK-net, in earthquake data in engineering seismology. *Geotechnical & Geological Earthquake Engineering*, *14*, 167–186. https://doi.org/10.1007/978-94-007-0152-6_12
- Banville, S., & Langley, R. B. (2010). Instantaneous cycle-slip correction for real-time PPP applications navigation. *Journal of the Institute of Navigation*, *57*(4), 325–334. <https://doi.org/10.1002/j.2161-4296.2010.tb01786.x>
- Benedetti, E., Branzanti, M., Biagi, L., Colosimo, G., Mazzoni, A., & Crespi, M. (2014). Global Navigation Satellite Systems seismology for the 2012 $M_w 6.1$ Emilia earthquake: Exploiting the VADASE algorithm. *Seismological Research Letters*, *85*(3), 649–656.
- Bock, Y., Melgar, D., & Crowell, B. W. (2011). Real-time strong-motion broadband displacements from collocated GPS and accelerometers. *Bulletin of the Seismological Society of America*, *101*(6), 2904–2925. <https://doi.org/10.1785.0120110007>
- Böse, M., Allen, R. M., Brown, H. M., Cua, G. B., Hauksson, E., Heaton, T., ... CISEN EEW Group (2012). CISEN ShakeAlert—An earthquake early warning demonstration system for California. In F. Wenzel & J. Zschau (Eds.), *Early warning for geological disasters* (Chap. 3, pp. 49–69). Berlin Heidelberg New York: Springer.
- Carranza, M., Buforn, E., Colombelli, S., & Zollo, A. (2013). Earthquake early warning for southern Iberia: A P wave threshold-based approach. *Geophysical Research Letters*, *40*, 4588–4593. <https://doi.org/10.1002/grl.50903>
- Colombelli, S., Caruso, A., Zollo, A., Festa, G., & Kanamori, H. (2015). A P wave-based, on-site method for earthquake early warning. *Geophysical Research Letters*, *42*, 1390–1398. <https://doi.org/10.1002/2014GL063002>
- Crowell, B. W., Melgar, D., Bock, Y., Haase, J. S., & Geng, J. (2013). Earthquake magnitude scaling using seismogeodetic data. *Geophysical Research Letters*, *40*, 6089–6094. <https://doi.org/10.1002/2013GL058391>
- Dach, R., Brockmann, E., Schaer, S., Beutler, G., Meindl, M., Prange, L., ... Ostini, L. (2009). GNSS processing at CODE: Status report. *Journal of Geodesy*, *83*(3–4), 353–365. <https://doi.org/10.1007/s00190-008-0281-2>
- Dach, R., Lutz, S., Walser, P., & Fridez, P. (2015). *Bernese GNSS Software Version 5.2*. Astronomical Institute, Bern, Switzerland: University of Bern. <https://doi.org/10.7892/boris.72297>
- Dimer de Oliveira, F. (2012). Can we trust earthquake cluster detection tests? *Geophysical Research Letters*, *39*, L17305. <https://doi.org/10.1029/2012GL052130>
- Dziewonski, A. M., & Anderson, D. L. (1981). Preliminary reference earth model. *Physics of the Earth and Planetary Interiors*, *25*(4), 297–356. [https://doi.org/10.1016/0031-9201\(81\)90046-7](https://doi.org/10.1016/0031-9201(81)90046-7)
- Ekström, G., Nettles, M., & Dziewonski, A. (2012). The global CMT project 2004–2010: Centroid-moment tensors for 13,017 earthquakes. *Physics of the Earth and Planetary Interiors*, *200–201*, 1–9. <https://doi.org/10.1016/j.pepi.2012.04.002>
- Espinosa-Aranda, J. M., Cuéllar, A., Rodríguez, F. H., Frontana, B., Ibarrola, G., Islas, R., & García, A. (2011). The seismic alert system of Mexico (SASMEX): Progress and its current applications. *Soil Dynamics and Earthquake Engineering*, *31*(2), 154–162. <https://doi.org/10.1016/j.soildyn.2010.09.011>
- Ge, M., Gendt, G., Rothacher, M., Shi, C., & Liu, J. (2008). Resolution of GPS carrier-phase ambiguities in precise point positioning (PPP) with daily observations. *Journal of Geodesy*, *82*(7), 389–399. <https://doi.org/10.1007/s00190-007-0187-4>
- Geng, J., & Bock, Y. (2013). Triple-frequency GPS precise point positioning with rapid ambiguity resolution. *Journal of Geodesy*, *88*(1), 95–97. <https://doi.org/10.1007/s00190-013-0667-7>
- Häbelring, S., Rothacher, M., Zhang, Y., Clinton, J. F., & Geiger, A. (2015). Assessment of high-rate GPS using a single-axis shake table. *Journal of Geodesy*, *89*(7), 697–709. <https://doi.org/10.1007/s00190-015-0808-2>

- Herring, T. A., King, R. W., & McClusky, S. M. (2015). *Introduction to GAMIT/GLOBK Release 10.6*. Cambridge: Massachusetts Institute of Technology.
- Hoshiba, M., & Iwakiri, K. (2011). Initial 30 seconds of the 2011 of the Pacific coast of Tohoku earthquake ($M_w9.0$) - amplitude and τ_c for magnitude estimation for earthquake early warning. *Earth Planets Space*, 63(7), 553–557. <https://doi.org/10.5047/eps.2011.06.015>
- Hoshiba, M., Iwakiri, K., Hayashimoto, N., & Shimoyama, T. (2011). Outline of the 2011 off the Pacific coast of Tohoku earthquake ($M_w9.0$)—Earthquake early warning and observed seismic intensity. *Earth Planets Space*, 63(7), 547–551. <https://doi.org/10.5047/eps.2011.05.031>
- Houlié, N., Dreger, D., & Kim, A. (2014). GPS source solution of the 2004 Parkfield earthquake. *Scientific Reports*, 4, 3646.
- Houlié, N., Occhipinti, G., Blanchard, T., Shapiro, N., Lognonne, P., & Murakami, M. (2011). New approach to detect seismic surface waves in 1 Hz-sampled GPS time series. *Scientific Reports*, 4(1), 44. <https://doi.org/10.1038/srep03646>
- Kanamori, H. (2005). Real-time seismology and earthquake damage mitigation. *Annual Review Earth and Planetary Science*, 33(1), 195–214. <https://doi.org/10.1146/annurev.earth.33.092203.122626>
- Kelevitz, K., Houlié, N., Giardini, D., & Rothacher, M. (2017). Performance of high-rate GPS waveforms at long periods: Moment tensor inversion of the 2003 $M_w8.3$ Tokachi-Oki earthquake. *Bulletin of the Seismological Society of America*. <https://doi.org/10.1785/0120160338>
- Marsaglia, G., Tsang, W. W., & Wang, J. (2003). Evaluating Kolmogorov's distribution. *Journal of Statistical Software*, 8, 18.
- McNamara, D. E., & Buland, R. P. (2004). Ambient noise levels in the continental United States. *Bulletin of the Seismological Society of America*, 94(4), 1517–1527. <https://doi.org/10.1785/012003001>
- McNamara, D. E., Hutt, C. R., Gee, L. S., Benz, H. M., & Buland, R. P. (2009). A method to establish seismic noise baselines for automated station assessment. *Seismological Research Letters*, 80(4), 628–637. <https://doi.org/10.1785/gssrl.80.4.628>
- Meier, U., Shapiro, N. M., & Brenguier, F. (2010). Detecting seasonal variations in seismic velocities within Los Angeles basin from correlation of ambient seismic noise. *Geophysical Journal International*, 181, 985–996. <https://doi.org/10.1111/j.1365-246X.2010.04550.x>
- Melgar, D., Bock, Y., Sanchez, D., & Crowell, B. W. (2013). On robust and reliable automated baseline corrections for strong motion seismology. *Journal of Geophysical Research*, 118, 1177–1187. <https://doi.org/10.1002/jgrb.50135>
- Melgar, D., Crowell, B. W., Geng, J., Allen, R. M., Bock, Y., Riquelme, S., ... Ganas, A. (2015). Earthquake magnitude calculation without saturation from the scaling of peak ground displacement. *Geophysical Research Letters*, 42, 5197–5205. <https://doi.org/10.1002/2015GL064278>
- Michel, C., Kelevitz, K., Houlié, N., Edwards, B., Psimoulis, P., Su, Z., ... Giardini, D. (2017). The potential of high-rate GPS for strong ground motion assessment. *Bulletin of the Seismological Society of America*, 107(3). <https://doi.org/10.1785/0120160296>
- Miyazaki, S., Larson, K. M., Choi, K., Hikima, K., Koketsu, K., Bodin, P., ... Yamagawa, A. (2004). Modeling the rupture process of the 2003 September 25 Tokachi-Oki (Hokkaido) earthquake using 1-Hz GPS data. *Geophysical Research Letters*, 31, L21603. <https://doi.org/10.1029/2004GL021457>
- Momoh, J. A., & Ziebart, M. (2012). *Instantaneous cycle slips detection, code multipath mitigation and improved ionospheric correction for enhanced GPS single-frequency positioning*. Paper presented at 25th Int. tech. Meet. Of the satellite division of the Institute of Navigation, (ION GNSS 2012) (pp. 3097–3112). Portland, OR.
- Moore, M., Watson, C., King, M., McClusky, S., & Tregoning, P. (2014). Empirical modeling of site-specific errors in continuous GPS data. *Journal of Geodesy*, 88(9), 887–900. <https://doi.org/10.1007/s00190-014-0729-5>
- Moschas, F., Avallone, A., Saltogianni, V., & Stiros, S. C. (2014). Strong motion displacement waveforms using 10-Hz precise point positioning GPS: An assessment based on free oscillation experiments. *Earthquake Engineering and Structural Dynamics*, 43(12), 1853–1866. <https://doi.org/10.1002/eqe.2426>
- Nakamura, Y. (1988). *On the urgent earthquake detection and alarm system (UrEDAS)*. Paper Presented at 9th World Conference on Earthquake Engineering, Tokyo-Kyoto, Japan.
- Noda, S., Yamamoto, S., Sato, S., Iwata, N., Korenaga, M., & Ashiya, K. (2012). Improvement of back-azimuth estimation in real-time by using single station record. *Earth Planets Space*, 64(3), 305–308. <https://doi.org/10.5047/eps.2011.10.005>
- Olson, E. L., & Allen, R. M. (2005). The deterministic nature of earthquake rupture. *Nature*, 438(7065), 212–215. <https://doi.org/10.1038/nature04214>
- Ozawa, S., Nishimura, T., Suito, H., Kobayashi, T., Tobita, M., & Imakiire, T. (2011). Coseismic and postseismic slip of the 2011 magnitude-9 Tohoku-Oki earthquake. *Nature*, 475(7356), 373–376. <https://doi.org/10.1038/nature10227>
- Psimoulis, P., Houlié, N., Meindl, M., & Rothacher, M. (2015). Consistency of GPS and strong-motion records: Case study of $M_w9.0$ Tohoku-Oki earthquake. *Smart Structures and Systems*, 16(2), 347–366. <https://doi.org/10.12989/sss.2015.16.2.347>
- Psimoulis, P., Houlié, N., Michel, C., Meindl, M., & Rothacher, M. (2014). Long-period surface motion of the multi-patch $M_w9.0$ Tohoku-Oki earthquake. *Geophysical Journal International*, 199(2), 968–980. <https://doi.org/10.1093/gji/ggu302>
- Psimoulis, P., Pytharoulis, S., Karambalis, D., & Stiros, S. (2008). Potential of Global Positioning System (GPS) to measure frequencies of oscillations of engineering structures. *Journal of Sound and Vibration*, 318(3), 606–623. <https://doi.org/10.1016/j.jsv.2008.04.036>
- Rhie, J., & Romanowicz, B. (2004). Excitation of Earth's continuous free oscillations by atmosphere–ocean–seafloor coupling. *Nature*, 431(7008), 552–556. <https://doi.org/10.1038/nature02942>
- Rhie, J., & Romanowicz, B. (2006). A study of the relation between ocean storms and the Earth's hum. *Geochemistry, Geophysics, Geosystems*, 7, Q10004. <https://doi.org/10.1029/2006GC001274>
- Rocken, C., Melvart, L., Jonhson, J., Lukes, Z., Springer, T., Iwabuchi, T., & Cummins, S. (2011). *A new real-time global GPS and GLONASS precise point positioning correction service: Apex*. Paper presented at 24th Int. tech. Meet. Of the satellite division of the Institute of Navigation (ION GNSS 2011) (pp. 1825–1838). Portland, OR.
- Rydelek, P., & Horiuchi, S. (2006). Earth science: Is earthquake rupture deterministic? *Nature*, 442(7100), E5–E6. <https://doi.org/10.1038/nature04963>
- Smirnov, N. (1948). Table for estimating the goodness of fit of empirical distributions. *Annals of Mathematical Statistics*, 19, 279–281. <https://doi.org/10.1214/aoms/1177730256>
- Stiros, S. (2008). Errors in velocities and displacements deduced from accelerographs: An approach based on the theory of error propagation. *Soil Dynamics and Earthquake Engineering*, 28(5), 415–420. <https://doi.org/10.1016/j.soildyn.2007.07.004>
- United States Geological Survey, 2015. Preliminary finite fault results for the Apr 25, 2015 $M_w7.8$ 28.1300, 846500 earthquake (version 1). Retrieved from <https://earthquake.usgs.gov/earthquakes/eventpage/us20002926%23finite-fault>
- Webb, S. (2008). The Earth's hum: The excitation of earth normal modes by ocean waves. *Geophysical Journal International*, 174(2), 542–566. <https://doi.org/10.1111/j.1365-246X.2008.03801.x>
- Wright, T. J., Houlié, N., Hildyard, M., & Iwabuchi, T. (2012). Real-time, reliable magnitudes for large earthquakes from 1 Hz GPS precise point positioning: The 2011 Tohoku-Oki (Japan) earthquake. *Geophysical Research Letters*, 39, L12302. <https://doi.org/10.1029/2012GL051894>

- Wu, Y.-M., & Zhao, L. (2006). Magnitude estimation using the first three seconds *P*-wave amplitude in earthquake early warning. *Geophysical Research Letters*, 33, L16312. <https://doi.org/10.1029/2006GL026871>
- Zhao, Q., Sun, B., Dai, Z., Hu, Z., Shi, C., & Liu, J. (2015). Real-time detection and repair of cycle slips in triple-frequency GNSS measurements. *GPS Solutions*, 19(3), 381–391. <https://doi.org/10.1007/s10291-014-0396-2>
- Zollo, A., Colombelli, S., Elia, L., Emolo, A., Festa, G., Iannaccone, G., ... Gasperini, P. (2013). An integrated regional and on-site earthquake early warning system for southern Italy: Concepts, methodologies and performances. In J. Z. Friedemann Wenzel (Ed.), *Early Warning for Geological Disasters-Scientific Methods and Current Practice* (pp. 117–138). Berlin Heidelberg New York: Springer. https://doi.org/10.1007/978-3-642-12233-0_7